Quantifying time-variant travel time distribution by multi-fidelity model in hillslope under nonstationary hydrologic conditions

Rong Mao[1], Jimmy Jiao[1], Xin Luo[1], and Hailong Li[2]

[1]Department of Earth Sciences, The University of Hong Kong, P. R. China.
[2]School of Environmental Science and Engineering, Southern University of Science and Technology, Shenzhen, P.R. China

Correspondence: Jimmy Jiao (jjiao@hku.hk)

Abstract. The travel time distribution (TTD) is a lumped representation of groundwater discharge and solute export responding to rainfall. It reflects the mixing process of water parcels and solute particles of different ages and characterizes reactive transport progress in hillslope aquifers. As a result of the mixing process, groundwater leaving the system at a certain time is an integration of multiple water parcels of different ages from different historical rainfall events. Under nonstationary rainfall input condition, the TTD varies with transit groundwater flow, leading to the time-variant TTD. Most methods for estimating time-variant TTD are constrained by requiring either the long-term continuous hydrogeochemical data or the intensive computations. This study introduces a multi-fidelity model to overcome these limitations and evaluate time-variant TTD numerically. In this multi-fidelity model, groundwater age distribution model is taken as the high-fidelity model, and particle tracking model without random walk is taken as the low-fidelity model. Non-parametric regression by non-linear Gaussian process is applied to correlate the two models and then build up the multi-fidelity model. The advantage of the multi-fidelity model is that it combines the accuracy of high-fidelity model and the computational efficiency of low-fidelity model. Moreover, in groundwater and solute transport model with low Péclet number, as the spatial scale of the model increases, the number of particles required for multi-fidelity model is reduced significantly compared to random walk particle tracking model. The correlation between high and low-fidelity models is demonstrated in a one dimensional pulse injection case. In a two dimensional hypothetical model, convergence analysis indicates that the multi-fidelity model converges well when increasing the number of high-fidelity models. Error analysis also confirms the good performance of the multi-fidelity model.

1 Introduction

The travel time of water in a hillslope is defined as the time duration for a water parcel to travel from one location where rainfall enters the aquifer to another location where groundwater exits the aquifer. Distinct water parcels can have very different travel time due to the mixing processes in the hillslope. The travel time distribution (TTD) is a lumped probability density function that represents the probability distribution of travel time. If water parcels are sampled from hillslope outflow, the TTD of the water parcels is defined as the backward TTD (bTTD); if the water parcels are tracked from rainfall input, the TTD of the water parcels is defined as the forward TTD (fTTD). TTD encapsulates the hydrologic dynamic and solute transport processes into a mathematic function and helps to study the time-varying transport and reaction processes in the hillslope, such as the genesis

25   and transport of weathering products (Ameli et al., 2017; Maher, 2010, 2011) and the attenuation of contaminants (Queloz et al., 2015).

Based on the time-invariant assumption of TTD, many previous studies approximated the TTD by the Gamma (Γ) distribution or some other probability density functions (Hrachowitz et al., 2009, 2010; Kirchner et al., 2000; McGuire and McDonnell, 2006). The time-invariant TTD quantifies the yearly averaged behaviors of transport processes. However, when attempting to

30   explore the time variability of water and solute transport in hillslopes under nonstationary rainfall input condition, it is necessary to adopt the time-variant assumption of TTD. Hence, several theories and approaches have been developed in the last decade to study the time-variant TTD.

The age master equation in accompany with the StorAge Selection (SAS) function (Botter et al., 2011) is one of the fundamental theories for these approaches. The age master equation is a storage mass balance equation characterizing the evolution

35   of storage age, namely the residence time. In the age master equation, the backward TTD quantifies the loss of age-tagged storage, and the SAS function relates the RTD with backward TTD. The SAS function illustrates how water parcels of different ages are released from storage. It characterizes the selection preference during the outflow generation. There are three principal types of selection preference: selection preference for younger water, selection preference for older water and no selection preference. In transient flow systems, the time-variant SAS function indicates the internal variability of the hydrologic system,

40   such as the temporal variability of flow paths. If the SAS function and storage volume are known based on prior information, the time-variant TTDs can be calculated by solving the age master equation analytically (Botter et al., 2011). However, in most real cases, the SAS function is unknown and is inferred from observed tracers using the age master equation.

A common approach to calculate time-variant TTDs is by coupling the age master equation with observed tracer data (Benettin et al., 2015a, b, c, 2017, 2013; van der Velde et al., 2015). This approach requires long-term continuous records of

45   rainfall rate, discharge rate and concentrations of the conservative tracer in both rainfall and discharge water. The approach generally employs an inverse modelling scheme to infer parameters in the adopted SAS function and age master equation. The long-term time series data are used to calibrate the model. When the posterior distributions of model parameters are estimated, time-variant TTD can be derived immediately from the age master equation. However, in many real catchments and hillslopes, the long-term monitored solute concentrations are not available. This approach of solving the age master equation

50   mainly requires the information at the recharge and discharge boundaries and does not need to have extensive hydrogeological information inside the hillslope, so the approach cannot be used to study the internal factors controlling the time variation of TTD and storage selection process, such as the influence of permeability architecture and preferential flow.

In addition to the approach to infer TTD based on age master equation, (Harman and Kim, 2014) developed an approach to derive the time-variant TTD directly from the breakthrough curve (BTC) of tracers under periodic hydrologic condition. No

55   pre-assumption about the SAS function is needed in this approach. The time-variant TTD can be constructed by decomposing the overprinted BTC into the contributions of multiple input events. This approach has been applied to indoor experimental hillslope successfully to explore the transport variability and storage-dependent TTDs (Kim et al., 2016; Pangle et al., 2017). The periodic condition is easy to control in experimental hillslopes, but such a condition is rare in real-world hillslopes.

Hydrology and
Earth System
Sciences
Discussions

Open Access

EGU

Random walk particle tracking is another approach to simulate the time-variant travel time distribution. Given the hydroge-
ological properties and boundary conditions in hillslope, the flow field can be determined by solving the governing equation
of groundwater flow. A set of particles are released at the input boundary and are tracked thereafter. The movement of each
particle depends on the transient flow field and molecular diffusion and mechanical dispersion. The molecular diffusion and
mechanical dispersion are approximated by random walk scheme. Several studies utilized this approach to analyze the time-
variant travel time distributions and compared the results of the SAS function from numerical simulations with analytical SAS
functions (Ameli et al., 2016a, b, 2017; Danesh-Yazdi et al., 2018; Kaandorp et al., 2018; Yang et al., 2018). This approach
makes it convenient to study the relation between the internal variability of transport processes and time-variant TTD, such as
the variability of flow path and preferential flow. However, if the transport is strongly influenced by molecular diffusion and
mechanical dispersion indicating a low Péclet number, this approach requires releasing a large number of particles during each
input event to reduce the random noise when implementing the random walk scheme.

Time-variant travel time distribution can also be evaluated by groundwater age distribution model. This approach adds an
age dimension to the governing equation of groundwater and solute transport (Benettin et al., 2013; Ginn et al., 2009; Gomez
and Wilson, 2013; Massoudieh and Ginn, 2011; Massoudieh, 2013). In a three dimensional (3D) transient flow system, it is
challenging to solve the five dimensional (5D) partial differential equation to obtain the groundwater age distribution. The five
dimensions consist of three spatial dimensions, one age dimension and one time dimension. Even so, there are some methods to
solve this 5D equation. Ginn et al. (2009) solved this equation numerically by directly discretizing this equation in a 5D space,
but most current softwares or codes do not have the module to visualize and discretize the 5D space, let alone solve the 5D
equation. Gomez and Wilson (2013) solved this equation by tracking each rainfall input which requires solving breakthrough
curves for each rainfall event. Cornaton (2012) solved this equation numerically in a Laplace space. The advantage of this
groundwater age distribution model is that it is valid to depict advection-dispersion transport processes with any Péclet number.

In this study, a multi-fidelity model is proposed to quantify the time-variant TTD. It consists of two models with different
levels of fidelities. The high-fidelity model is the groundwater age distribution model, and the low-fidelity model is the particle
tracking model without considering random walk. Nonlinear Gaussian process regression method is applied to relate the high-
fidelity with low-fidelity models. Then, the 5D governing equation of groundwater and solute transport can be solved and time-
variant TTD can be calculated by the multi-fidelity model. The multi-fidelity model takes advantages of both the efficiency of
low-fidelity model and the accuracy of high-fidelity model, so it is easier to be implemented numerically in real-world aquifers
compared with previous methods especially for those aquifers with low Pécelt number and large spatial scale.

2 Theoretic framework of multi-fidelity model

The multi-fidelity model is designed to calculate TTD, RTD and SAS function by solving the equation of groundwater age
distribution. It combines the groundwater age distribution model and particle tracking model to evaluate the time-variant TTD
in a system. The two models which have different levels of fidelities will be introduced first.

2.1 Groundwater age distribution model

Due to the mixing process undergoing along groundwater flow lines, the groundwater or solutes sampled from a certain point is a mixture of constituents (e.g., groundwater, solutes, and suspended colloids) of various ages. The groundwater age distribution describes the portion of the constituent of a certain age τ at a point. The governing equation for groundwater age distribution

95 was primarily introduced by Ginn (1999) and is modified with variable saturation in this study as follows:

$$\frac{\partial \phi S_w \rho}{\partial t} + \frac{\partial \phi S_w \rho}{\partial \tau} = \nabla \cdot (\phi S_w D \cdot \nabla \rho) - \nabla \cdot (\boldsymbol{v} \rho) \tag{1}$$

where ϕ is porosity; S_w is water saturation; $\boldsymbol{v}$ is Darcy velocity; D is the diffusion coefficient including molecular diffusion and mechanical dispersion. $\rho(\boldsymbol{x}, t, \tau)$ is the age density function of a constituent at time t and point $\boldsymbol{x}$. If integrating $\rho(\boldsymbol{x}, t, \tau)$ along age-axis (τ-axis), the mass density $c(\boldsymbol{x}, t)$ of this constituent is obtained, that is,

100 $$c(\boldsymbol{x}, t) = \int_0^\infty \rho(\boldsymbol{x}, t, \tau) \mathrm{d}\tau \tag{2}$$

The definition of mass density is the ratio of mass to volume. If the concerned constituent is water, mass density is the water density and equal to $1 \, g/cm^3$; if the concerned constituent is solute, mass density is the solute concentration. Equation (1) describes the evolution of the age of groundwater in the system in Eularian method. The groundwater age distribution can be obtained by normalizing the age density function $\rho(\boldsymbol{x}, t, \tau)$ over the mass density $c(\boldsymbol{x}, t)$, that is, $\frac{\rho(\boldsymbol{x}, t, \tau)}{c(\boldsymbol{x}, t)}$. The transport of mass

105 density obeys the rules described in the following equation (3), i.e. the advection-dispersion equation (ADE) for conservative solute transport:

$$\frac{\partial \phi S_w c}{\partial t} = \nabla \cdot (\phi S_w D \cdot \nabla c) - \nabla \cdot (\boldsymbol{v} c) \tag{3}$$

If groundwater flow is under steady state condition, the groundwater age distribution is a time-invariant distribution, i.e., $\rho(\boldsymbol{x}, t, \tau) = \rho(\boldsymbol{x}, 0, \tau)$ and $c(\boldsymbol{x}, t) = c(\boldsymbol{x}, 0)$, and the governing equation for groundwater age distribution (equation (1)) be-

110 comes:

$$\frac{\partial \phi S_w \rho}{\partial \tau} = \nabla \cdot (\phi S_w D \cdot \nabla \rho) - \nabla \cdot (\boldsymbol{v} \rho) \tag{4}$$

Equation (4) is similar to the ADE in equation (3) and can be solved using the methods to solve the ADE.

However, if groundwater flow is under unsteady state condition, the groundwater age distribution is a time-variant distribution, which means that the age density function $\rho(\boldsymbol{x}, t, \tau)$ and groundwater age distribution $\frac{\rho(\boldsymbol{x}, t, \tau)}{c(\boldsymbol{x}, t)}$ varies in both clock-time

115 t and field point $\boldsymbol{x}$. As a result, the groundwater age distribution can only be obtained by solving equation (1) which is a 5D equation with 3 space dimensions, 1 clock-time dimension and 1 age dimension. Equation (1) resolves the evolution of age distribution of a constituent in the system, and it is challenging to solve equation (1) either analytically or numerically.

Referring to the study of Gomez and Wilson (2013), one approach to obtain the numerical solution (i.e. $\rho(\boldsymbol{x}, t, \tau)$) of equation (1) is to decompose equation (1) into a series of independent ADEs. Each ADE has a different initial condition. In this approach,

Hydrology and
Earth System
Sciences
Discussions

Open Access

EGU

120 the input time η is introduced as a new variable to replace the age variable τ, such that:

$$\eta = t - \tau \tag{5}$$

$$\rho'(\boldsymbol{x}, t, \eta) = \rho(\boldsymbol{x}, t, \tau) \tag{6}$$

$$\frac{\partial \rho}{\partial \tau} = -\frac{\partial \rho'}{\partial \eta}; \quad \frac{\partial \rho}{\partial t} = \frac{\partial \rho\prime}{\partial t} + \frac{\partial \rho\prime}{\partial \eta} \tag{7}$$

Then equation (1) becomes:

125 $$\frac{\partial \phi S_w \rho'}{\partial t} = \nabla \cdot (\phi S_w D \cdot \nabla \rho') - \nabla \cdot (\boldsymbol{v}\rho') \tag{8}$$

where ρ' is age density function which represents the mass density of water entering the system at the time η as is shown in equation (6). Equation (8) is similar to the ADE, i.e., equation (3), but they have different physical meanings, because the variable ρ' depends on the input time η. Equation (8) must be solved for each input event occurred during the study period.

The BTC at the discharge boundary for a certain input time η can be derived from ρ':

130 $$BTC(\tau, \eta) = \int_{\partial \Omega} (\phi S_w \boldsymbol{v}\rho' - \phi S_w D \cdot \nabla \rho') \cdot \boldsymbol{n} \mathrm{d}\Sigma_{discharge} \tag{9}$$

where τ is the travel time defined as the age at the discharge boundary $\Sigma_{discharge}$. Therefore, equation (9) quantifies the mass flux along the discharge boundary for a certain travel time. Since TTD can be decomposed into a series of overprinted BTCs induced by different pulse injections (Harman and Kim, 2014), the time-variant TTDs at the outflow boundary can be constructed by assembling these sets of BTCs.

135 The advantage of this approach is that it reduces the dimension of the problem by changing the age variable τ into the input time variable η, because the water from the same input event must have the same age. However, in real problems, the model should be simulated for each input event to acquire a good resolution of age distribution. Therefore, in this study, the ADE for a certain input event is defined as high-fidelity model. This high-fidelity model is required to run only a few times for several input events in multi-fidelity model to capture the trend of the variation of age distributions and ensure the multi-fidelity model 140 unbiased.

2.2 Particle tracking model

Particle tracking is a popular approach to model the time-variant TTDs based on Lagrangian advective transport. As all particles are tagged with their own ages, the time-variant TTDs can be evaluated by counting the particles at the discharge boundary. To simulate the molecular diffusion and mechanical dispersion of solutes, it is necessary to add an random walk velocity to the 145 advection velocity for each particle. Yang et al. (2018) used the random walk particle tracking model to evaluate time-variant TTD in an agricultural catchment. However, the random walk particle tracking model may suffer from random noise when the number of particles released is insufficient to simulate the diffusion and mechanical dispersion behaviors. This random noise is even inevitable if using particle tracking method in the problems with large space scales. Therefore, in this multi-fidelity model, random walk velocity is excluded from particle velocity, and the particle tracking without considering random walk

150 is defined as the low-fidelity model. Particles are released at the recharge boundary during each rainfall event. Each particle represents a certain volume of water parcels based on the rainfall infiltration rate. As the random walk velocity is not included in the low-fidelity model, the random noise disappears, and the number of particles decreases drastically. Generally, as the scale of the model becomes larger, more particles are required to be released in random walk particle tracking model, so the number of particles in the low fidelity model decreases even more.

2.3 Analytical theorem for one dimensional scenario

Prior to establishing the multi-fidelity model, the correlation between particle tracking model and ADE is investigated analytically in 1D condition. In the particle tracking model, a particle represents a pulse signal of water or solute entering the domain at a certain injection time. The transport of the pulse signal in 1D domain is studied to illustrate the relation between the two models. Assume the advection velocity is a constant in the entire domain, the transport of the pulse injection can be expressed

160 as:

$$\frac{\partial \rho'}{\partial t} = -v \frac{\partial \rho'}{\partial x} \tag{10}$$

with the initial condition:

$$\rho' = M\delta(x - x_0) \tag{11}$$

where ρ' is defined in equation (6); $\delta(x - x_0)$ is the Dirac delta function which represents a pulse signal ocurred at the point

165 x_0; M is the intensity of the pulse signal, namely the input mass density. The solution of equation (10) is explicative:

$$\rho' = M\delta(x - vt - x_0) \tag{12}$$

when considering molecular diffusion and mechanical dispersion in ADE, equation (10) is manifested as:

$$\frac{\partial \rho'}{\partial t} = D \frac{\partial^2 \rho'}{\partial x^2} - v \frac{\partial \rho'}{\partial x} \tag{13}$$

The analytical solution of equation (13) with respect to the initial condition of equation (11) at infinite domain is:

170 $$\rho' = \frac{M}{\sqrt{4\pi Dt}} e^{-\frac{(x - vt - x_0)^2}{4Dt}} \tag{14}$$

Comparing solution (14) with solution (12), it can be found that as the parameter D goes to zero, the bell-shape curve of solution (14) converges to the Dirac delta function of solution (12), that is,

$$\lim_{D \to 0} \frac{M}{\sqrt{4\pi Dt}} e^{-\frac{(x - vt - x_0)^2}{4Dt}} = M\delta(x - vt - x_0) \tag{15}$$

This is consistent with the relation between the two governing equations: equation (13) has an additional diffusion term com-

175 pared with equation (10). Therefore, no matter under what boundary conditions, the solution of equation (13) will always converge to equation (12) when D approaches zero.

Theoretically, a mapping is capable of being setting up between the solutions (12) and (14) for a given hydrogeological model if the diffusion parameter D is known. This is the theoretical foundation of the multi-fidelity model.

2.4 Multi-fidelity model for arbitrary 2D/3D models

In the approach proposed by Gomez and Wilson (2013), the equation of groundwater age distribution is decomposed into a series of ADE to track the transport of water from each rainfall event separately, because the water from the same rainfall event always has the same age. The ADE can be solved either by numerical simulation or by random walk particle tracking model. For random walk particle tracking model, the problem of random noise has already been discussed in the previous section. For the numerical simulation method, it should be run separately for each rainfall input, or a different chemical species need to be assigned for each rainfall event to differentiate the transport among different rainfall events. Specifically, if there are 200 rainfall events in one year, the numerical simulation should be run 200 times, or 200 different chemical species should be assigned for this 200 rainfall events. Moreover, the water from two rainfall events which are closed to each other may have similar transport process, so the simulation for all rainfall event is redundant.

The aim of the multi-fidelity model is to quantify the time-variant TTD through equation (1), i.e., the equation of groundwater age distribution. This multi-fidelity model is implemented by four steps: firstly decomposing the equation of ADEs into a series of ADE, secondly solving these ADEs through particle tracking without random walk (low-fidelity model), thirdly solving several ADEs by numerical simulation (high-fidelity model), and finally establishing multi-fidelity model for the relation between the BTCs from low-fidelity model and high-fidelity model and calculating the time-variant TTD from the BTCs of multi-fidelity model.

The results of the low-fidelity model is the solution of equation (16) derived from omitting the diffusion term in equation (8):

$$\frac{\partial \phi S_w \rho'}{\partial t} = -\nabla \cdot (\boldsymbol{v} \rho') \tag{16}$$

Based on the nonlinear correlation between equations (13) and (10) described previously, the solution of equation (8) can be obtained by mapping from the low-fidelity model to the high-fidelity model. The mapping is expressed as a nonlinear autoregressive model:

$$f_H(t,\eta) = g\left(f_L(t,\eta), t, \eta\right) \tag{17}$$

where $f_H(t,\eta)$ is the solution of ADE model which has high-fidelity, $f_L(t,\eta)$ is the solution of particle tracking model without conidering random walk which has low-fidelity, and g represents the nonlinear mapping. Given a certain hydrogeological model, the nonlinear mapping g only depends on the diffusion coefficient D, but the mathematical form of the nonlinear mapping can vary with different hydrogeological models. The mapping of equation (17) can also be applied to link the cumulative breakthrough curves (cBTC) between two models of different levels of fidelity, because the evaluation of BTC through equation (9) and the transformation of BTC to cBTC are both linear operations with respect to age mass density ρ'. Therefore, in this study, $f_H(t,\eta)$ is the cBTC from ADE model, and $f_L(t,\eta)$ is the cBTC from particle tracking model without random walk. To ensure the mapping accommodate any hydrogeological model, non-parametric regression with Gaussian processes (GPs) (Raissi et al., 2017; Zhang et al., 2018) is adopted to build up the multi-fidelity model. Let $\boldsymbol{m} = [f_L(t,\eta), t, \eta]$, then the

nonlinear mapping $g\left(f_L(t,\eta), t, \eta\right)$ in equation (17) can be written as $g(\boldsymbol{m})$ and is assigned to a GP prior:

$$g(\boldsymbol{m}) \sim \mathcal{GP}\left(f_H | 0, k\left(\boldsymbol{m}, \boldsymbol{m}'; \boldsymbol{\theta}\right)\right) \tag{18}$$

where $\mathcal{GP}$ represents the Gaussian process; 0 is the prior mean value; $k\left(\boldsymbol{m}, \boldsymbol{m}'; \boldsymbol{\theta}\right)$ is the kernel function with hyper-parameters $\boldsymbol{\theta}$. The kernel function in GP prior quantifies the pairwise correlation between f_{Hi} and f_{Hj} and leads to a symmetric covariance matrix $K_{ij} = K_{ji} = k\left(\boldsymbol{m}_i, \boldsymbol{m}_j; \boldsymbol{\theta}\right)$ between the points $(\boldsymbol{m}_i, f_{Hi})$ and $(\boldsymbol{m}_j, f_{Hj})$. If $\boldsymbol{m}_i$ and $\boldsymbol{m}_j$ are close to each other, the correlation between f_{Hi} and f_{Hj} will be high. The term on the right hand side of equation (18) is the GP prior which means the probability distribution of f_H is a Gaussian distribution with mean value 0 and variance $k\left(\boldsymbol{m}, \boldsymbol{m}'; \boldsymbol{\theta}\right)$.

With reference to the work of Perdikaris et al. (2017), the kernel function is expressed as:

$$k\left(\boldsymbol{m}, \boldsymbol{m}'; \boldsymbol{\theta}\right) = k_1\left((t,\eta), (t,\eta)'; \boldsymbol{\theta}_1\right) \cdot k_2\left(f_L, f_L'; \boldsymbol{\theta}_2\right) + k_3\left((t,\eta), (t,\eta)'; \boldsymbol{\theta}_3\right) \tag{19}$$

In equation (19), the kernel function $k\left(\boldsymbol{m}, \boldsymbol{m}'; \boldsymbol{\theta}\right)$ consists of three components: k_1 denotes the correlation dependence of the modeling time and input time, k_2 denotes the correlation dependence of the results of low-fidelity model, and k_3 denotes the correlation of the regression errors. Each correlation is quantified by a squared exponential covariance function which means that the covariance between f_{Hi} and f_{Hj} decreases exponentially as the distance between $\boldsymbol{m}_i$ and $\boldsymbol{m}_j$ decreases:

$$k_p\left(\boldsymbol{x}, \boldsymbol{x}', \boldsymbol{\theta}_p\right) = \sigma_p^2 e^{-\frac{1}{2}\sum_{q=1}^{d} w_{p,q}\left(x_q - x_q'\right)^2} \tag{20}$$

where $\boldsymbol{\theta}_p = \left[\sigma_p^2, (w_{p,q})_{q=1}^d\right]$, and $\boldsymbol{\theta}$ is the vector of hyper-parameters for the covariance function k_p ($p=1,2,3$) in equation (19), σ_p^2 is the variance parameter, $(w_{p,q})_{q=1}^d$ are the automatic relevance determination weights, and $\boldsymbol{x}$ is a d-dimensional input vector which can be (t,η) or f_L in equation (19).

The vector of hyper-parameters $\boldsymbol{\theta}_p$ ($p=1,2,3$) in equation (19) determines the performance of the mapping. With a given regression data set $(M_{in}, \boldsymbol{F}_H) = (\boldsymbol{m}_i, f_{Hi})_{i=1\ldots n}$ obtained from particle tracking model and ADE model, the hyper-parameters $\Theta = [\boldsymbol{\theta}_1, \boldsymbol{\theta}_2, \boldsymbol{\theta}_3]$ can be estimated by minimizing the negative marginal log-likelihood:

$$-\log p\left(\boldsymbol{F}_H | M_{in}, \Theta\right) = \frac{1}{2}\boldsymbol{F}_H^T K^{-1}\boldsymbol{F}_H + \frac{1}{2}\log|K| + \frac{n}{2}\log 2\pi \tag{21}$$

where $\boldsymbol{F}_H^T = [f_{H1}, f_{H2}, f_{H3}, \ldots]$, $M_{in} = [\boldsymbol{m}_1, \boldsymbol{m}_2, \boldsymbol{m}_3, \ldots]$; K is the covariance matrix which is evaluated by equation (20) based on the input data $\boldsymbol{m}_i$ and hyper-parameters Θ; n is the number of pairs of data for regression.

Once the hyper-parameters are determined based on the regression data set $(M_{in}, \boldsymbol{F}_H)$, the value of f_{Hnew} at new point $\boldsymbol{m}_{new}$ can be predicted. The prediction is implemented by computing the posterior distribution $p\left(f_{Hnew} | \boldsymbol{F}_H\right)$. Referring to the definition of GP, the joint distribution of f_{Hnew} and $\boldsymbol{F}_H$ is expressed as a joint Gaussian distribution:

$$\begin{bmatrix} f_{Hnew} \\ \overrightarrow{F}_H \end{bmatrix} \sim \mathcal{N}\left(\begin{bmatrix} 0 \\ \overrightarrow{0} \end{bmatrix}, \begin{bmatrix} K_{Hnew-Hnew} & K_{Hnew-H} \\ K_{H-Hnew} & K_{H-H} \end{bmatrix}\right) \tag{22}$$

where K_{x-y} represents the covariance between x and y. Then, the posterior distribution is exactly the marginal distribution of the joint Gaussian distribution:

$$f_{Hnew} = g\left(\overrightarrow{m}_{new}\right) \big| \overrightarrow{F}_H \sim \mathcal{N}\left(\mu, \sigma^2\right) \tag{23}$$

where the predicted mean is $\mu = K_{Hnew-H}^T K_{H-H}^{-1} \boldsymbol{F}_H$, and the predicted variance is $\sigma_{out}^2 = K_{Hnew-Hnew} - K_{Hnew-H}^T K_{H-H}^{-1} K_{Hnew-H}$.

In this way, the BTCs for all rainfall events can be inferred from the mapping based on the solution of the particle tracking model without random walk. For a complex hydrogeological system, it is difficult to derive the mapping analytically, so the non-parametric regression model is employed to estimate the mapping. Overall, the number of rainfall events considered in

245 ADE model is reduced compared with the groundwater age distribution model (Gomez and Wilson, 2013); and the number of particles released is reduced significantly compared with the random particle tracking model (Yang et al., 2018). The multi-fidelity model also makes the evaluation of time-variant TTD simpler to be implemented compared with the approach that evaluates time-variant TTD numerically in Laplace space (Cornaton, 2012). There is a tradeoff between the computational cost and accuracy. Larger the size of regression data set is, the more accurate the regression will be, but the computational cost will

250 also be higher. The problem of how to determine the size of regression data set will be discussed in the illustrative example.

2.5 Evaluation of the time variant TTD and SAS function

Referring to the definition of forward TTD of water (fTTD), each BTC can be transformed to a fTTD by normalizing it with the total rainfall recharge volume. Let $\overrightarrow{p}_T(\eta, \tau)$ represents the fTTD conditional to rainfall event occurred at time η, then

$$\overrightarrow{p}_T(\eta, \tau) = \frac{BTC(\tau, \eta)}{P(\eta)} \tag{24}$$

255 where τ is the age known as travel time at the outflow site, $P(\eta)$ is the rainfall recharge volume at time η, $BTC(\tau, \eta)$ is the BTC of water which is input at time η. Equation (24) displays a one-to-one mapping between the BTC and fTTD. The fTTD quantifies the portion of water leaving the system at time t within the same rainfall event.

To study the time-variant behavior of the storage selection process, backward TTD of water (bTTD) and residence time distribution of water (RTD) are evaluated to explore the dynamic storage selection process. Similar to the evaluation of fTTD,

260 bTTD can be calculated by normalizing the BTCs with the discharge rate as follows,

$$\overleftarrow{p}_T(t, \tau) = \frac{BTC(\tau, t - \tau)}{Q(t)} \tag{25}$$

where $\overleftarrow{p}_T(t, \tau)$ is the bTTD. Given a certain time t in equation (25), the evaluation of bTTD requires the BTCs before the time t. This is because the water in the hillslope discharging at the time t comes from the rainfall occurred before the time t.

Up to now, most studies employ BTC to calculate fTTD and bTTD directly (Harman and Kim, 2014; Kim et al., 2016), but

265 few studies calculate RTD by the BTC. As the results obtained from multi-fidelity model are a set of BTCs conditional on each rainfall event, it is necessary to put forward a method to calculate RTD using BTCs. The cBTC is defined as:

$$cBTC(t, \eta) = \int_{\eta}^{t} BTC(t_{out}, \eta)\, dt_{out} \tag{26}$$

The cBTC $cBTC(t, \eta)$ characterizes the total volume of water or solutes from the same rainfall event at the discharge boundary before the time t. Therefore, the water or solutes that still remains in the system at the time t is equal to $P(\eta) - cBTC(t, \eta)$.

270   The RTD $p_s(t, \tau)$ describes the age distribution in storage calculated as follows:

$$p_s(t, t - \eta) = \frac{P(\eta) - cBTC(t, \eta)}{\sum_{\eta < t}(P(\eta) - cBTC(t, \eta))} \tag{27}$$

where $P(\eta)$ is the total volume of rainfall which is infiltrated at the time η. By assembling these cBTCs, the denominator in equation (27) represents the total storage volume at time t.

Having calculated the bTTD and RTD, the storage selection (SAS) function can be quantified according to its definition.

275   To characterize the time-variant behaviors of storage selection process conveniently, the fractional SAS function (fSAS) is calculated based on the results of bTTD and RTD (van der Velde et al., 2012). Because there is a one-to-one mapping between the groundwater residence time (groundwater age) and cumulative RTD, fSAS function is defined as a function of cumulative RTD and time:

$$\omega_Q(t, P_s) = \frac{\overleftarrow{p}_T(t, \tau(P_s))}{p_s(t, \tau(P_s))} \tag{28}$$

280   where $\omega_Q(t, P_s)$ is the fSAS and $P_s(t, \tau)$ is the cumulative RTD. Many studies employ beta distribution to quantify this fSAS function (van der Velde et al., 2012; Danesh-Yazdi et al., 2016).

3   Illustrative example: a hypothetical model with nonstationary rainfall input

A hypothetical 2D hillslope model is setup to illustrate the performance of the multi-fidelity model. With nonstationary rainfall recharge applied on the upper boundary of the model, the time-variant TTD and SAS function are calculated. The errors of

285   TTD and SAS function are compared between multi-fidelity model and low-fidelity model.

3.1   Model setup

As shown in Figure 1, the geometry of the model is a quadrangle that is 100 m long in the x-axis direction. The thickness of the model at the left and right boundaries are 8 m and 5 m, respectively. The bottom of domain represents boundary of the impermeable bedrock. The depth of the fresh bedrock head increases from the toe to the top of the hillslope. This model is based

290   on a real hillslope of igneous rock in Hong Kong under subtropic climate condition. The groundwater at up-slope generally has a lower solute concentration and a higher water-rock reaction rate compared with the groundwater at the down-slope (Braun et al., 2016; Rempe and Dietrich, 2014). This leads to the wedge-shaped profile of weathered rock zone.

The numerical simulation of ADE model and particle tracking model without random walk are implemented in the software COMSOL Multiphysics (COMSOL AB, 2018). Three modules in COMSOL are employed, namely Richards' equation

295   module, transport of dilute species in porous media module, and mathematical particle tracing module.

In Richards' equation module, hydraulic head and Darcy velocity are solved to couple with the other two modules. The left boundary and bottom boundary are no-flow boundaries, the right boundary is a fix-head boundary with hydraulic head equal to 4.5 meters. The top boundary is a time-variant rainfall infiltration boundary. Figure 2 shows the variation of 2-year nonstationary rainfall volume per day with 2728.5 mm rainfall volume in total during the first year and 2678.5 mm during the
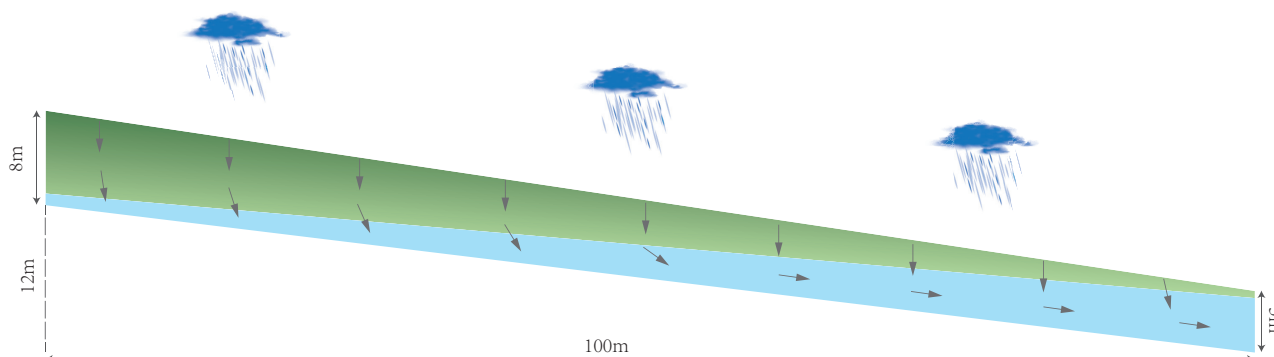
Figure 1. A hypothetic two dimensional modeling domain based on a hillslope of weathered igneous rock

second year, which are taken from the real rainfall record of Hong Kong Observatory in 2016 and 2017. The rainfall infiltration rate is set to be 0.2. The modeling period is 10046 days. The 2-year rainfall will be repeated every two years.
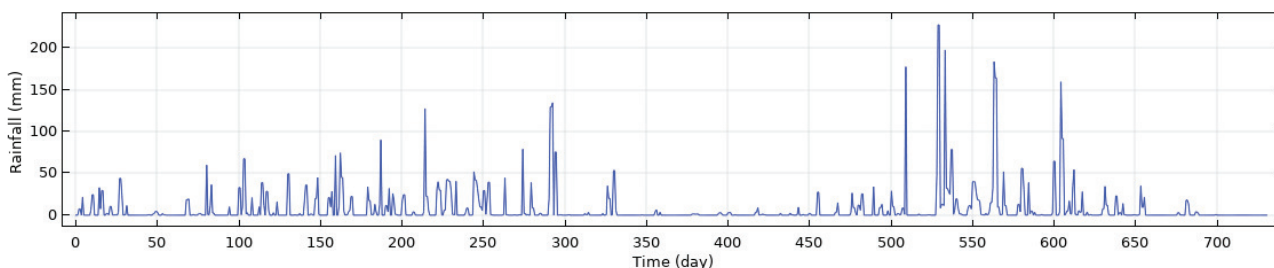
Figure 2. Two-year rainfall for recharge boundary

As the goal of this study is to explore the time-variant TTD and storage selection process in hillslope, the spatial heterogeneity of hydrogeological properties is ignored and only one layer with constant hydraulic conductivity is considered in this hypothetic model. The detailed hydraulic parameters are shown in Table 1. Theoretically, the initial condition for Richards' equation can be arbitrary, but in order to reach a periodic quasi-steady state rapidly, the initial condition is set to be:

$$h(x) = -0.15x + 19.5 \tag{29}$$

where the initial hydraulic gradient is equal to the slope gradient. After running a spin-up period of 4 years, the solution of Richards' equation reaches a periodic quasi-steady state. Then the solution of this module is coupled with the other two modules through Darcy velocity to further solve for the BTCs.

The transport of dilute species in the porous media module in COMSOL is used to solve for the groundwater age distribution model. This is because equation (8) has the same mathematical form as the solute transport equation. Therefore, the mass density in equation (8) can be regarded as a solute concentration while modeling. As is discussed in the section 2.1, this module should be run for each single rainfall event independently to obtain BTCs. The advection velocity required in this

Hydrology and
Earth System
Sciences
Discussions
Open Access

EGU

Table 1. Hydraulic parameters applied in Richards' equation module

Parameters	K	D_m	ϕ	S_r	α	n	l
Values	$7.5 \times 10^{-6} m/s$	$1 \times 10^{-9} m^2/s$	0.3	0.05	1.5	1.5	0.5

K: hydraulic conductivity

D_m: molecular diffusion coefficient

ϕ: porosity

S_r: Residual saturation

α, n, l: parameters in VG model

Longitudinal mechanical dispersivity: $a_L = 0.05$m

Transverse mechanical dispersivity: $a_T = 0.01$m

module is the Darcy velocity which has been solved in the first module. The left and bottom boundaries are no-flux boundary

315 for transport. The right boundary is a free outflow boundary meaning that the outflow of water and solute is dominated by advection and the diffusion term is equal to zero. This kind of outflow boundary condition is widely used in the transport problems where no constrain of solute concentration exists at the outflow boundary. The top boundary is a given flux boundary dependent on the rainfall intensity. Since rainfall is the only source in the model, the initial condition of the mass density is zero in the whole domain. Then the BTCs are evaluated at the right outflow boundary according to equation (9). The BTCs obtained

320 in this module are taken as the solution of high-fidelity model, because this model is based on the real physical process with very limited assumptions.

The mathematical particle tracing module in COMSOL is employed to solve for the BTCs without considering molecular diffusion and mechanical dispersion. The particles are released along the hillslope surface uniformly during rainfall. The number of particles released at the upper boundary is the same for each rainfall event. Each particle represents a certain volume

325 of water parcels depending on the rainfall intensity. As the diffusion effect is not considered in this module, the movements of these particles are deterministic based on the groundwater velocity. A particle counter is set at the discharge boundary to keep counting the arriving particles to evaluate the BTCs. The BTCs calculated in this module are taken as the solution of low-fidelity model, because the solution is biased against the high-fidelity model due to the absence of molecular diffusion and mechanical dispersion effect.

330 Figure 3 compares the result at day 1050 calculated from high-fidelity model with the result calculated from low-fidelity model qualitatively. The red dots represent the distribution of water parcels in low-fidelity model. The colored contour plot shows the spatial distribution of age density function $\rho(\boldsymbol{x}, t, \tau)$ (unit: kg/m^3) in high-fidelity model. These two results displayed in figure 3 are for the water entering the system during the rainfall event occurred at day 165. In figure 3, the age density function spreads around the red dots due to molecular diffusion and mechanical dispersion, and this is consistent with the analytical 1D

335 correlation of equation (15).
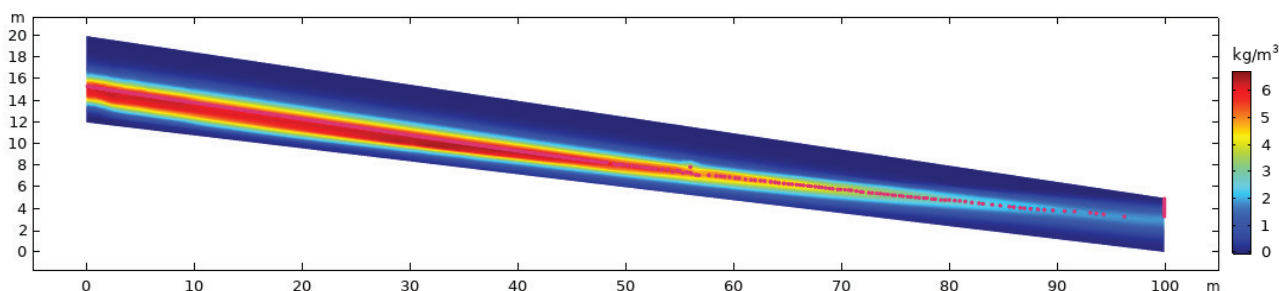
Figure 3. Comparison of the results between particle tracking model and solute transport model at time=1050 day. The results are for the water entering the system during the rainfall event occurred at day 165.

3.2 Selecting regression data set for multi-fidelity model

Having set up these modules in COMSOL, there are two more factors affecting the result of the multi-fidelity model and should be specified before running the multi-fidelity model, that is, (1) the selection of specific high-fidelity models for regression data set and (2) the number of selected high-fidelity models in regression data set. To study how these two factors affect the results, 340 correlation, error and convergence analysis are implemented. The nonlinear regression with Gaussian process used in multi-fidelity model is realized in python using the Gpy package (GPy, since 2012).

There are many methods available to assist in selecting the high-fidelity models for regression data set. In this study, the distance method is employed and is fully described by Scheidt and Caers (2009); Josset et al. (2015). Specifically, as the distance of selected parameters between high-fidelity models becomes short, the results of multi-fidelity model are closer to 345 the results of high-fidelity models. In high-fidelity models, the selected parameter is the time when rainfall occurred. If the two rainfall events are very close, the two BTCs at the discharge boundary will be similar due to the similarity of hydraulic conditions. Therefore, the selection of the data set for regression is based on the 'distance' between the rainfall time, i.e. the interval between two rainfall events. In this hypothetical model, there are 290 rainfall events every 2 years, and the rainfall events are selected successively from 290 events with a constant distance. The cBTCs calculated from high-fidelity models 350 within the selected rainfall events make up the regression data set for regression.

The distance among the rainfall events is used to control the number of high-fidelity models in regression data set. Therefore, it is vital to determine a reasonable distance, and this will be discussed in the following error analysis and convergence analysis. To evaluate the error of regression and study the convergence of the multi-fidelity model, the high-fidelity model is solved for all the 290 rainfall events intensively to generate the test data set. Practically, only error analysis is required during the 355 implementation of multi-fidelity model, so the size of test data set can be much smaller .

The 2-norm error of a certain BTC reflects the overall deviations of the predicted BTC from the BTC in the test data set, and is calculated below:

$$\|e\|_2 = \sqrt{\frac{1}{N}\sum_{n=1}^{N}|y_n - y(t_n)|^2} \tag{30}$$

13

where $\|e\|_2$ is the 2-norm error of a certain BTC, N is the number of points in the BTC, y_n and $y(t_n)$ are the points in BTC

360   calculated by multi-fidelity model and high-fidelity model respectively. The 2-norm error is used to quantify the goodness-of-fit of the calculated BTC by multi-fidelity model.

In the convergence analysis, the size of the regression data set increases by shortening the interval between rainfall events. Figure 4 shows the relation between the 2-norm errors of BTCs calculated by multi-fidelity model and the interval between rainfall events.
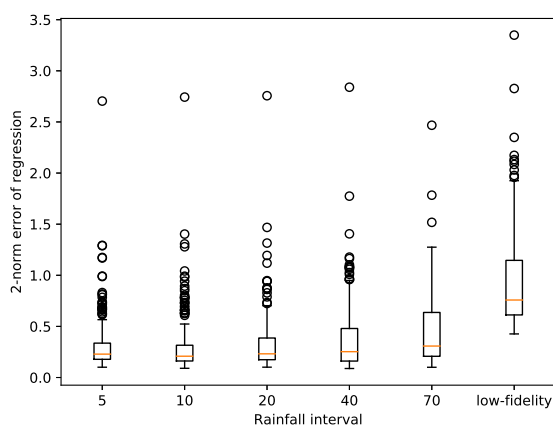
Figure 4. Box plot of the 2-norm errors of BTCs calculated by multi-fidelity model with respect to rainfall interval. The last box is the 2-norm errors of BTCs calculated by low-fidelity model.

365   As shown in Figure 4, the goodness-of-fit improves as the interval among rainfall events shortens. This confirms that multi-fidelity model converges as the size of regression data set increases.

Then an interval of 10 rainfall events is employed to calculate the predicted errors of cBTCs in details. The predicted error is defined as the difference value between the predicted BTC and the BTC evaluated by high-fidelity model. Figure 5 compares the predicted errors for all 290 realizations between the multi-fidelity model and low-fidelity model. Each grey curve in Figure

370   5 represents the predicted errors of a BTC. The mean predicted errors in Figure 5a are very close to zero, which indicates that the predicted curves are unbiased and the selected high-fidelity models with the interval of 10 days for regression data set is representative of all high-fidelity BTCs. However, the mean predicted errors in Figure 5b are biased against the negative value. The biased errors are identified as the system errors. It implies that the solute concentration in discharge predicted by particle tracking without random walk is generally smaller than that predicted by high-fidelity model, because except for the advection

375   process, the molecular diffusion and mechanical dispersion can also transport solute from recharge boundary to discharge boundary.

The goodness-of-fit for model with 'distance' of the interval 10 is shown in Figure 6 directly. It can be seen that most of the predicted cBTCs match the high-fidelity model well. Also, these inconsistencies between predicted cBTCs and cBTCs
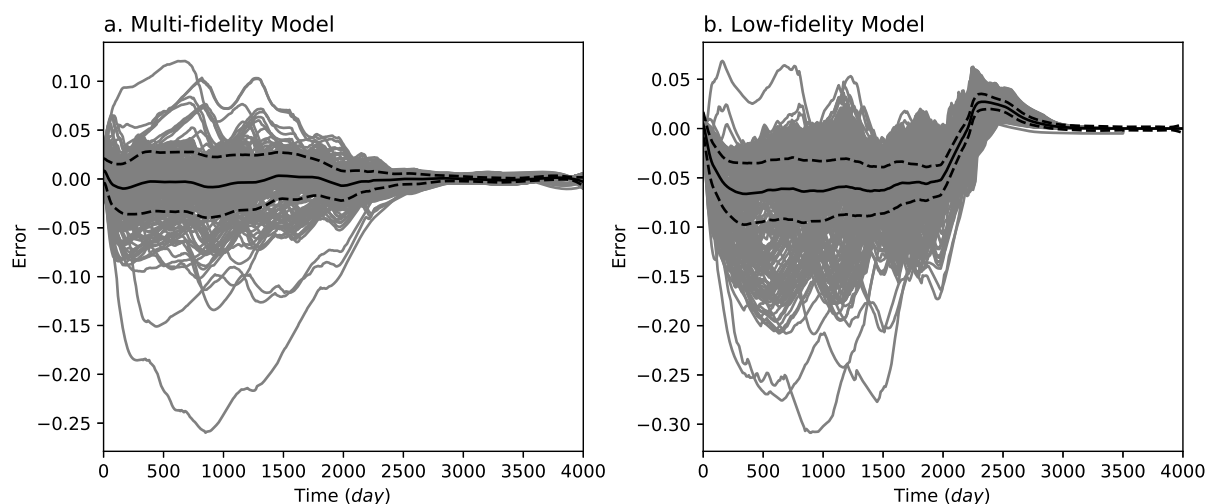
Figure 5. Predicted error (grey line) of BTCs for all 290 rainfall events of the multi-fidelity model (sub-figure a) and low-fidelity model (sub-figure b), the mean error (black solid line) and the standard deviation (black dash line) are also shown.

evaluated from high fidelity model in day 510 and day 654 are acceptable, because the overall errors shown in figure 5 are
380 unbiased and decreased. These predicted cBTCs are further applied to evaluate the time-variant TTD and SAS. The interval of 10 rainfall events is recommended for the application of the multi-fidelity model in other problems, because the interval of 10 rainfall events is equivalent to about one-month interval in wet season and about two-or-three month interval in dry season.

### 3.3 Errors of time-variant bTTD, RTD and fSAS function

With reference to equations (25) and (27), time-variant bTTD and RTD are obtained based on the cBTC, while fSAS function
385 is calculated based on bTTD and RTD using equation (28). The 2-norm errors of bTTD, RTD and fSAS function calculated by multi-fidelity model are compared with the 2-norm errors calculated by low-fidelity model. The results of bTTD, cumulative bTTD, RTD, cumulative RTD and fSAS function from different models in two years are presented in figures 7, 8 and 9. These curves are colored by storage volume to illustrate how the bTTD and RTD change with the system storage. Similar to the calculation of 2-norm errors of BTC, the calculations of 2-norm errors of bTTD, cumulative bTTD, RTD, cumulative RTD and
390 fSAS function are also based on equation (30). In the box plots of 2-norm errors in figures 7, 8 and 9, the 2-norm errors of bTTD, cumulative bTTD, RTD, cumulative RTD and fSAS function calculated by high-fidelity model are reduced significantly compared with those calculated by low-fidelity model.

In figures 7 and 8, the bTTD and cumulative TTD are significantly distinctive among the multi-fidelity model, high-fidelity model and low-fidelity model, but the difference of the RTD and cumulative RTD among the three models is not identifiable.
395 This phenomenon is ascribed to the difference of kinetics (i.e., molecular diffusion and mechanical dispersion) of water parcels
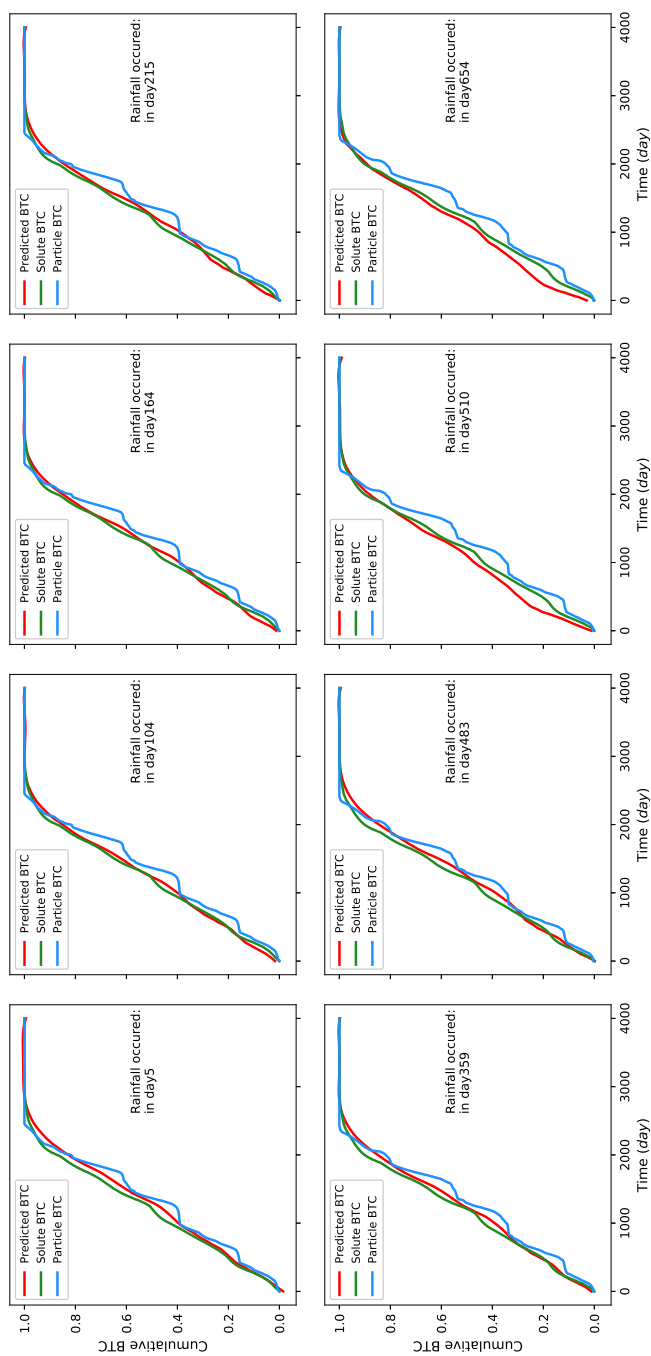
Figure 6. The comparison of predicted cBTCs (multi-fidelity model) with the solute cBTC (high-fidelity model) and the particle cBTCs (low-fidelity model) on different rainy days.
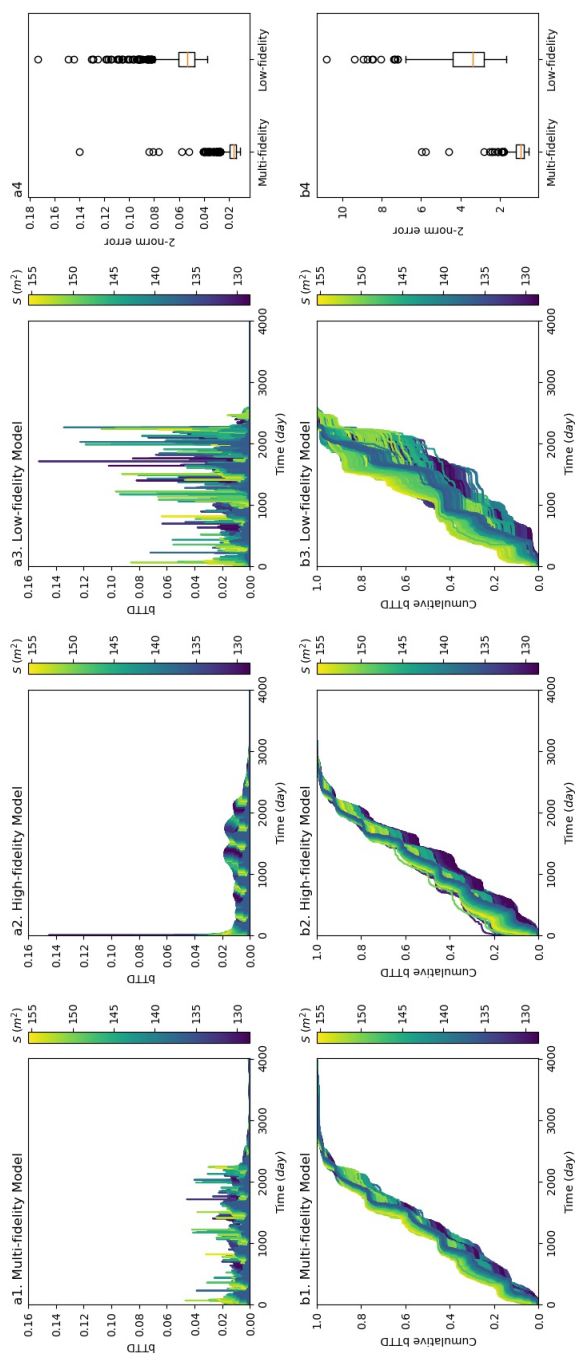
Figure 7. (a) Time-variant bTTDs colored by their transit storages and calculated from multi-fidelity model (a1), high-fidelity model (a2) and low-fidelity model (a3); (b) Time-variant cumulative bTTDs colored by their transit storages and calculated from multi-fidelity model (b1), high-fidelity model (b2) and low-fidelity model (b3); (a4) and (b4) are the box plots of 2-norm errors of bTTDs and cumulative bTTDs respectively.
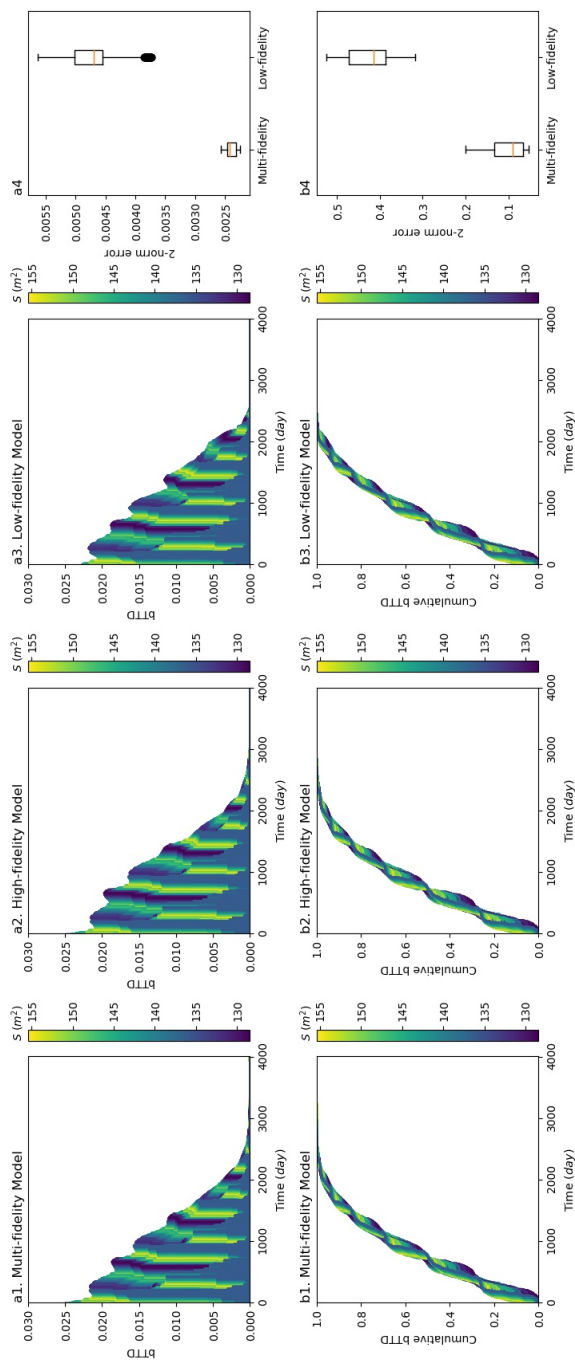
Figure 8. (a) Time-variant RTDs colored by their transit storages and calculated from multi-fidelity model (a1), high-fidelity model (a2) and low-fidelity model (a3); (b) Time-variant cumulative RTDs colored by their transit storages and calculated from multi-fidelity model (b1), high-fidelity model (b2) and low-fidelity model (b3); (a4) and (b4) are the box plots of 2-norm errors of RTDs and cumulative RTDs respectively.

Hydrology and
Earth System
Sciences
Discussions
Open Access
EGU
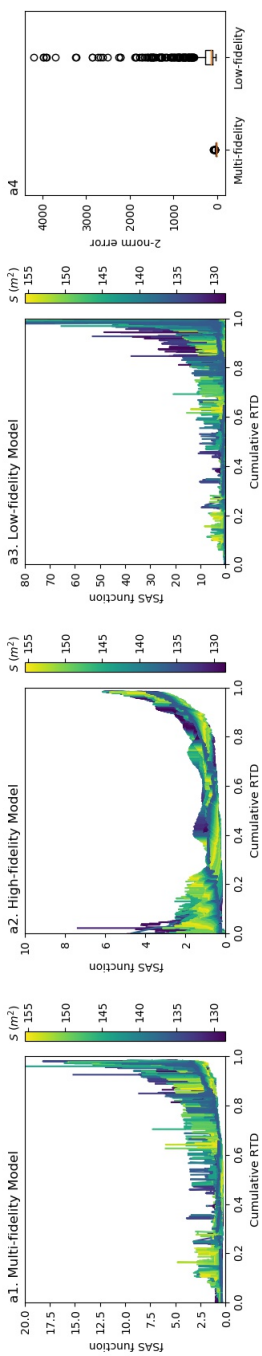
Figure 9. Time-variant fSAS functions colored by their transit storages and calculated from multi-fidelity model (a1), high-fidelity model (a2) and low-fidelity model (a3); (a4) is the box plot of 2-norm errors of fSAS functions calculated by multi-fidelity model and low-fidelity model.

and solutes among the three models. As the goal of study is to introduce a method to calculate time-variant TTD, the influences of molecular diffusion and mechanical dispersion on time-variant TTD and RTD will be discussed in future studies.

4 Conclusions

The TTD provides basic information on travel time of water and solute flowing through the system. The travel time of water
400 characterizes the transport and reaction progresses in the hillslope system. Several methods had been introduced to estimate TTD in previous studies, such as the age master equation model, particle tracking model, groundwater age distribution model, etc. However most of these methods have their limitations. This study develops a new method to calculate the TTD and SAS function directly, and the errors are compared with the particle tracking method without considering random walk.

This multi-fidelity model combines the ADE model (high-fidelity model) and particle tracking model without random walk
405 (low-fidelity model) by non-linear Gaussian process regression. It reduces the computational time of high-fidelity model and improves the accuracy of low-fidelity model. For the development of multi-fidelity model, the goodness-of-fit of the multi-fidelity model increases with the size of regression data set, i.e., the number of high-fidelity models. In the convergence analysis, a criterion and a feasible method are put forward for multi-fidelity model to determine the size of regression data set and select high-fidelity models for regression. The errors of cBTCs calculated from multi-fidelity model is unbiased, but these
410 errors calculated from particle tracking model are biased against negative values due to the absence of molecular diffusion and mechanical dispersion. The 2-norm errors of bTTD, cumulative bTTD, RTD, cumulative RTD and fSAS function calculated by multi-fidelity model are also reduced significantly compared with the 2-norm errors calculated by low-fidelity model. Meanwhile, as the spatial scale of the model increases, the number of particles required for multi-fidelity model reduces dramatically compared with the number of particles required for random walk particle tracking method. Therefore, in the
415 large-scale water and solute transport model with a low Péclet number, the multi-fidelity model is better than the groundwater age distribution model and random walk particle tracking model to calculate time-variant TTD numerically.

Author contributions. Rong Mao, Jiu Jimmy Jiao, Xin Luo and Hailong Li designed the research, Rong Mao performed the research and
420 wrote the paper.

References

425   Ameli, A. A., Amvrosiadi, N., Grabs, T., Laudon, H., Creed, I. F., McDonnell, J. J., and Bishop, K.: Hillslope permeability architecture controls on subsurface transit time distribution and flow paths, Journal of Hydrology, 543, 17–30, https://doi.org/10.1016/j.jhydrol.2016.04.071, 2016a.

Ameli, A. A., McDonnell, J. J., and Bishop, K.: The exponential decline in saturated hydraulic conductivity with depth: a novel method for exploring its effect on water flow paths and transit time distribution, Hydrological Processes, 30, 2438–2450,
430   https://doi.org/10.1002/hyp.10777, 2016b.

Ameli, A. A., Beven, K., Erlandsson, M., Creed, I. F., McDonnell, J. J., and Bishop, K.: Primary weathering rates, water transit times, and concentration-discharge relations: A theoretical analysis for the critical zone, Water Resources Research, 53, 942–960, https://doi.org/10.1002/2016wr019448, 2017.

Benettin, P., Rinaldo, A., and Botter, G.: Kinematics of age mixing in advection-dispersion models, Water Resources Research, 49, 8539–
435   8551, https://doi.org/10.1002/2013wr014708, 2013.

Benettin, P., Bailey, S. W., Campbell, J. L., Green, M. B., Rinaldo, A., Likens, G. E., McGuire, K. J., and Botter, G.: Linking water age and solute dynamics in streamflow at the Hubbard Brook Experimental Forest, NH, USA, Water Resources Research, 51, 9256–9272, https://doi.org/10.1002/2015wr017552, 2015a.

Benettin, P., Kirchner, J. W., Rinaldo, A., and Botter, G.: Modeling chloride transport using travel time distributions at Plynlimon, Wales,
440   Water Resources Research, 51, 3259–3276, https://doi.org/10.1002/2014wr016600, 2015b.

Benettin, P., Rinaldo, A., and Botter, G.: Tracking residence times in hydrological systems: forward and backward formulations, Hydrological Processes, 29, 5203–5213, https://doi.org/10.1002/hyp.10513, 2015c.

Benettin, P., Soulsby, C., Birkel, C., Tetzlaff, D., Botter, G., and Rinaldo, A.: Using SAS functions and high-resolution isotope data to unravel travel time distributions in headwater catchments, Water Resources Research, 53, 1864–1878,
445   https://doi.org/doi:10.1002/2016WR020117, 2017.

Botter, G., Bertuzzo, E., and Rinaldo, A.: Catchment residence and travel time distributions: The master equation, Geophysical Research Letters, 38, n/a–n/a, https://doi.org/10.1029/2011gl047666, 2011.

Braun, J., Mercier, J., Guillocheau, F., and Robin, C.: A simple model for regolith formation by chemical weathering, Journal of Geophysical Research: Earth Surface, 121, 2140–2171, https://doi.org/10.1002/2016jf003914, 2016.

450   COMSOL AB: COMSOL Multiphysics v. 5.4., www.comsol.com., stockholm, Sweden, 2018.

Cornaton, F. J.: Transient water age distributions in environmental flow systems: The time-marching Laplace transform solution technique, Water Resources Research, 48, https://doi.org/10.1029/2011wr010606, 2012.

Danesh-Yazdi, M., Foufoula-Georgiou, E., Karwan, D. L., and Botter, G.: Inferring changes in water cycle dynamics of intensively managed landscapes via the theory of time-variant travel time distributions, Water Resources Research, 52, 7593–7614,
455   https://doi.org/10.1002/2016wr019091, 2016.

Danesh-Yazdi, M., Klaus, J., Condon, L. E., and Maxwell, R. M.: Bridging the gap between numerical solutions of travel time distributions and analytical storage selection functions, Hydrological Processes, 32, 1063–1076, https://doi.org/10.1002/hyp.11481, 2018.

Ginn, T. R.: On the distribution of multicomponent mixtures over generalized exposure time in subsurface flow and reactive transport: Foundations, and formulations for groundwater age, chemical heterogeneity, and biodegradation, Water Resources Research, 35, 1395–
460   1407, https://doi.org/doi:10.1029/1999WR900003, 1999.

Ginn, T. R., Haeri, H., Massoudieh, A., and Foglia, L.: Notes on Groundwater Age in Forward and Inverse Modeling, Transport in Porous Media, 79, 117–134, https://doi.org/10.1007/s11242-009-9406-1, 2009.

Gomez, J. D. and Wilson, J. L.: Age distributions and dynamically changing hydrologic systems: Exploring topography-driven flow, Water Resources Research, 49, 1503–1522, https://doi.org/10.1002/wrcr.20127, 2013.

465 GPy: GPy: A Gaussian process framework in python, http://github.com/SheffieldML/GPy, since 2012.

Harman, C. J. and Kim, M.: An efficient tracer test for time-variable transit time distributions in periodic hydrodynamic systems, Geophysical Research Letters, 41, 1567–1575, https://doi.org/10.1002/2013gl058980, 2014.

Hrachowitz, M., Soulsby, C., Tetzlaff, D., Dawson, J. J. C., Dunn, S. M., and Malcolm, I. A.: Using long-term data sets to understand transit times in contrasting headwater catchments, Journal of Hydrology, 367, 237–248, https://doi.org/10.1016/j.jhydrol.2009.01.001, 2009.

470 Hrachowitz, M., Soulsby, C., Tetzlaff, D., Malcolm, I. A., and Schoups, G.: Gamma distribution models for transit time estimation in catchments: Physical interpretation of parameters and implications for time-variant transit time assessment, Water Resources Research, 46, https://doi.org/10.1029/2010wr009148, 2010.

Josset, L., Ginsbourger, D., and Lunati, I.: Functional error modeling for uncertainty quantification in hydrogeology, Water Resources Research, 51, 1050–1068, https://doi.org/doi:10.1002/2014WR016028, 2015.

475 Kaandorp, V. P., Louw, P. G. B., Velde, Y., and Broers, H. P.: Transient Groundwater Travel Time Distributions and Age-Ranked Storage-Discharge Relationships of Three Lowland Catchments, Water Resources Research, 54, 4519–4536, https://doi.org/doi:10.1029/2017WR022461, 2018.

Kim, M., Pangle, L. A., Cardoso, C., Lora, M., Volkmann, T. H. M., Wang, Y., Harman, C. J., and Troch, P. A.: Transit time distributions and StorAge Selection functions in a sloping soil lysimeter with time-varying flow paths: Direct observation of internal and external transport 480 variability, Water Resources Research, 52, 7105–7129, https://doi.org/10.1002/2016wr018620, 2016.

Kirchner, J. W., Feng, X., and Neal, C.: Fractal stream chemistry and its implications for contaminant transport in catchments, Nature, 403, 524, 2000.

Maher, K.: The dependence of chemical weathering rates on fluid residence time, Earth and Planetary Science Letters, 294, 101–110, https://doi.org/10.1016/j.epsl.2010.03.010, 2010.

485 Maher, K.: The role of fluid residence time and topographic scales in determining chemical fluxes from landscapes, Earth and Planetary Science Letters, 312, 48–58, https://doi.org/10.1016/j.epsl.2011.09.040, 2011.

Mao, R.: Codes and dataset used in the manuscript entitled "Quantifying time-variant travel time distribution by multi-fidelity model in hillslope under nonstationary hydrologic conditions", https://doi.org/10.5281/zenodo.5195801, 2021.

Massoudieh, A.: Inference of long-term groundwater flow transience using environmental tracers: A theoretical approach, Water Resources 490 Research, 49, 8039–8052, https://doi.org/10.1002/2013wr014548, 2013.

Massoudieh, A. and Ginn, T. R.: The theoretical relation between unstable solutes and groundwater age, Water Resources Research, 47, https://doi.org/10.1029/2010wr010039, 2011.

McGuire, K. J. and McDonnell, J. J.: A review and evaluation of catchment transit time modeling, Journal of Hydrology, 330, 543–563, https://doi.org/10.1016/j.jhydrol.2006.04.020, 2006.

495 Pangle, L. A., Kim, M., Cardoso, C., Lora, M., Meira Neto, A. A., Volkmann, T. H. M., Wang, Y., Troch, P. A., and Harman, C. J.: The mechanistic basis for storage-dependent age distributions of water discharged from an experimental hillslope, Water Resources Research, 53, 2733–2754, https://doi.org/doi:10.1002/2016WR019901, 2017.

Perdikaris, P., Raissi, M., Damianou, A., Lawrence, N. D., and Karniadakis, G. E.: Nonlinear information fusion algorithms for data-efficient multi-fidelity modelling, Proc Math Phys Eng Sci, 473, 20160 751, https://doi.org/10.1098/rspa.2016.0751, 2017.

500 Queloz, P., Bertuzzo, E., Carraro, L., Botter, G., Miglietta, F., Rao, P. S. C., and Rinaldo, A.: Transport of fluorobenzoate tracers in a vegetated hydrologic control volume: 1. Experimental results, Water Resources Research, 51, 2773–2792, https://doi.org/10.1002/2014wr016433, 2015.

Raissi, M., Perdikaris, P., and Karniadakis, G. E.: Inferring solutions of differential equations using noisy multi-fidelity data, Journal of Computational Physics, 335, 736–746, https://doi.org/10.1016/j.jcp.2017.01.060, 2017.

505 Rempe, D. M. and Dietrich, W. E.: A bottom-up control on fresh-bedrock topography under landscapes, Proceedings of the National Academy of Sciences, 111, 6576–6581, https://doi.org/10.1073/pnas.1404763111, 2014.

Scheidt, C. and Caers, J.: Representing spatial uncertainty using distances and kernels, Mathematical Geosciences, 41, 397, 2009.

van der Velde, Y., Torfs, P. J. J. F., van der Zee, S. E. A. T. M., and Uijlenhoet, R.: Quantifying catchment-scale mixing and its effect on time-varying travel time distributions, Water Resources Research, 48, https://doi.org/10.1029/2011wr011310, 2012.

510 van der Velde, Y., Heidbüchel, I., Lyon, S. W., Nyberg, L., Rodhe, A., Bishop, K., and Troch, P. A.: Consequences of mixing assumptions for time-variable travel time distributions, Hydrological Processes, 29, 3460–3474, https://doi.org/10.1002/hyp.10372, 2015.

Yang, J., Heidbüchel, I., Musolff, A., Reinstorf, F., and Fleckenstein, J. H.: Exploring the Dynamics of Transit Times and Subsurface Mixing in a Small Agricultural Catchment, Water Resources Research, https://doi.org/10.1002/2017wr021896, 2018.

Zhang, J., Man, J., Lin, G., Wu, L., and Zeng, L.: Inverse modeling of hydrologic systems with adaptive multi-fidelity Markov chain Monte
515 Carlo simulations, Water Resources Research, https://doi.org/10.1029/2018wr022658, 2018.